A Mesoscale Budget Study of Cumulus Convection

ALAN L. McNAB[1] AND ALAN K. BETTS

Department of Atmospheric Science, Colorado State University, Fort Collins 80523

(Manuscript received 25 November 1977, in final form 10 April 1978)

ABSTRACT

Water and energy budgets are presented for four broad classes of summertime cumulus convection. The budgets are calculated from National Hail Research Experiment rawinsonde data. The convection classifications are based on radar and precipitation data. A derivation of the budget equation is presented in order to point out two terms that are related to the rapid time changes and large horizontal gradients that sometimes occur over the budget area.

Weak, moderate and precipitating classes of convection produced apparent sources of water and energy that are generally similar to the results of other budget studies based on oceanic and/or tropical data. The results for the developing class of convection demonstrate that a cloud storage term must be included when studying convection that is rapidly changing from weak to moderate or precipitating.

1. Introduction

The total water and energy input of cumulus clouds to a mesoscale circulation cannot be assessed by direct measurements taken on the scale of individual clouds. Consequently, convective transports of water and energy over mesoscale or larger areas are often determined by a budget approach. A budget calculation for a given volume is simply the algebraic sum of the measured inflow, outflow and storage of water or energy set equal to a source term plus a contribution due to flows that are not resolved by the measurements. The unresolved flows are assumed to be due to cumulus convection in the given volume.

Although a budget calculation is straightforward to carry out, its interpretation is not straightforward. The time and space resolution of the input data and the amount of averaging used in the budget calculation are of basic importance in the interpretation of individual budget terms. The interpretation of mesoscale budgets is further complicated by the possibility of strong interactions or feedbacks between the large-scale environment terms and the small-scale convection terms.

This paper presents a mesoscale budget study of water and energy transports associated with summertime cumulus convection over the National Hail Research Experiment (NHRE) area. The mesoscale environment of the convection over the NHRE area has considerably different characteristics (e.g., greater horizontal gradients and time changes) than the environments of most of the previous budget studies of convection. Consequently, this calculation provides a useful addition to the current store of budget results. During several periods the amount of clouds over the NHRE area changed so rapidly that a cloud storage term was included in the budget calculation. This term has been neglected in previous budget studies. The calculated budgets are stratified and averaged according to a simple radar description of the convection. This radar classification of convection is more detailed than most of the convection descriptions used in other budget studies. The additional detail aids in the interpretation of the budget results. Finally, an interpretation of one of the budget calculations is presented in terms of a simple model. The use of a model is a key step in understanding the relations between cumulus convection and mesoscale circulations.

2. Data

a. Data network

The budget calculations are based on 14 days of high-density rawinsonde measurements taken during the 1973 summer NHRE. These budgets are related to radar echo and precipitation occurrence data within the NHRE area.

Rawinsondes were released approximately simultaneously from the five NHRE sites (Fig. 1) at 2–3 h intervals from 1100 to 1800 LST. As pointed out by Fankhauser (1969), a mesoscale analysis of rawinsonde data should account for sonde rise time and downwind drift. The NHRE sondes typically drifted 5 km downstream at 500 mb and 40 km at 100 mb. The extreme drift distances at 100 mb are 5 and 65 km. The paths traced out by two successive sondes usually fall within 2 km of each other at the 500 mb level and 6 km of each other at the 100 mb level. The data along one

[1] Present affiliation: Department of Meteorology, The Pennsylvania State University, University Park 16802.

0027-0644/78/1317-1331$07.50

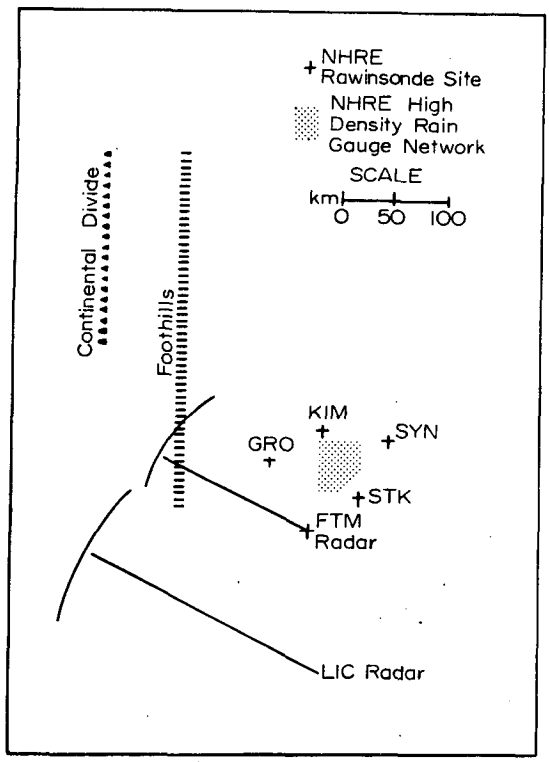

FIG. 1. National Hail Research Experiment (NHRE) data area.

sounding path are not valid at one single time because of sonde rise time. The balloons reached the 500 mb level about 10 min after launch and the 100 mb level about 50 min after launch. Also, the five launch times for one set of ascents sometimes differed by as much as 30 min. A set of "simultaneous" ascents were used as data only when at least four of the five rawinsondes reached 175 mb. Two such successive sets of sonde data are needed to make one budget calculation. A total of 39 data intervals are used for the budget calculations.

Radar and precipitation data have also kindly been supplied by the NHRE personnel. The precipitation data are obtained from the high-density raingage network within the NHRE area [119 sites spaced approximately 5–10 km apart (see Fig. 1)]. Radar data consist of photographs of the Ft. Morgan PPI radar scope, plus additional PPI photographs obtained from the Limon radar (Fig. 1). The overall time resolution of the radar data is severely limited due to missing data due to a large variety of causes. Also, the height resolution of the radar data is very coarse because there were not many elevation angle changes for scans that covered the entire NHRE area. The final radar data set consists of PPI photographs of the entire NHRE area at half-hour to hour intervals.

b. Data reduction

There are two general parts to the data reduction procedure in this study: 1) the rawinsonde wind, temperature and mixing ratio data are interpolated in time and space so that they can be used in the water and energy budget calculations; and 2) the radar and precipitation data are simplified into four broad categories useful in describing the general type (or intensity) of convection occurring during each budget calculation interval.

The first step of the rawinsonde data reduction is a vertical interpolation of each sounding to evenly spaced σ levels ($\sigma = P/P_{stc}$). A fine vertical spacing of $\Delta\sigma = 0.01$ (8–9 mb) is used to retain the contact point temperature information even though the wind data are not available at this spacing. The data at each level are then linearly interpolated in time with data from the corresponding level of the previous ascent. The results of these interpolations are sets of four or five soundings (depending on whether four or five balloons reached the 175 mb level) valid at a common time. Each data volume defined by such a set of soundings tilts downwind. Fig. 2 schematically pictures a typical downwind drift of five sondes. The data from each of the five sondes has been interpolated in time with the previous five sondes (not shown in Fig. 2) so that all data for each level and for each sonde are valid at one single time.

The budget equation derived in Section 3 requires data from a series of vertically stacked areas. As shown in Fig. 2, the choice of the budget area is not at all clear because of the substantial sonde drift. In this research the budget area is centered over the approximate midpoint of the overlapping data area. See Fig. 2 for definition of this "overlapping" area and its midpoint C. The extent of the budget area is then defined as a 50 km radius circle centered at this midpoint.

The data within this area are approximated as the following linear functions of horizontal position:

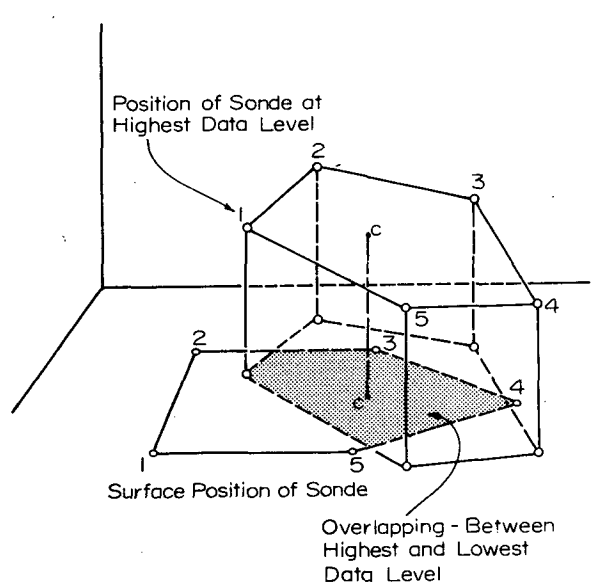

FIG. 2. Typical downwind drift of NHRE rawinsondes.

TABLE 1. Average absolute differences between original data and plane values.

σ	Δq (g kg^{-1})	ΔT (K)	ΔZ (m)	Δu (m s^{-1})	Δv (m s^{-1})
1.00	0.49	0.61	1.41	0.74	0.66
0.60	0.21	0.33	3.81	0.77	0.84
0.20	0.00	0.30	11.46	1.95	1.61

$\chi_i = a_i x + b_i y + c_i$. The subscript i refers to the various data obtained from the rawinsoundings ($\chi_i = u, v, q, z, T$) and the coefficients a_i, b_i and c_i are determined by doing a least-squares fit of the χ_i's measured at each of the four or five known balloon positions. A different set of coefficients is computed for each variable at each vertical data level. A good fit of the data to these planes is of fundamental importance in the budget analysis (see Section 3). The sample absolute differences presented in Table 1 are on the order of the measurement errors associated with the GMD-1a rawinsonde system, suggesting that u, v, q, T and z do vary linearly across the mesoscale data area. The algebraic averages are all less than 0.00 (in the units used).

Before the final set of rawinsonde data was determined, the vertical velocity $\pi\dot{\sigma}$ (π = surface pressure) profiles were calculated using the linear wind values in the continuity equation. The vertically integrated results showed unrealistic values of $\pi\dot{\sigma}$ on the order of 7×10^{-3} mb s^{-1} at the highest data levels ($\sim$120 mb). To remedy this a divergence adjustment technique developed by O'Brien (1970) and used by Fankhauser (1969, 1974) was used to force the $\pi\dot{\sigma}$ to zero at these highest data levels. In this technique the divergence is adjusted by an amount linearly proportional to height. The actual velocity components are adjusted by evenly dividing the divergence correction between the x slope of the u component and the y slope of the v component. After these adjustments are made the first part of the data reduction is complete. These final sets of data are used to calculate the resolved time changes and horizontal and vertical divergences of water and energy throughout the mesoscale budget volume. Vertical profiles of the sum of these resolved terms are related to the cumulus convection (see Section 4).

The second part of the data reduction is the simplification of the radar and precipitation observations to produce an additional description of the cumulus convection within the budget area. In contrast to the above budget description derived from the sonde data, the radar and precipitation data are used to present a more "physical" picture of the intensity or activity of the cumulus clouds within the budget area. Four categories of convective fields are defined: 1) weak suppressed, 2) weak developing, 3) moderate, 4) precipitating. The specific characteristics of these categories are presented in Table 2.

The weak suppressed category is comparable to the "undisturbed" BOMEX period discussed by Holland and Rasmusson (1973), Nitta and Esbensen (1974) and, Betts (1975); the "no echo" class of Ninomiay (1974); "region 8" (ridge region) of Reed and Recker (1971); and the "weak/absent" convective activity period of Augstein *et al.* (1973). The precipitating category is similar to the BOMEX "disturbed" period, Reed and Recker's (1971) "trough" category (categories 4 and 5) and Ninomiya's (1974) "echo cluster" period. Some comparisons of this category can also be made to two mesoscale budget analyses of thunderstorms (Fankhauser, 1969; Lewis, 1975) and to a composite mesoscale cumulonimbus budget (Betts, 1973). The weak developing and moderate categories are not particularly comparable to any single category mentioned above. It is likely that the type of cumulus clouds characteristic of these two categories were present in both the disturbed and undisturbed classes already noted.

Even though the four categories of this study are somewhat finer than other studies they are still quite broad. They involve only a distinction of whether or not precipitation and/or radar echoes were present

TABLE 2. Convection categories.

Category	Radar/precipitation characteristics of cumulus clouds	Number of budget intervals*
Weak suppressed	No observed precipitation No radar echoes during budget interval No radar echoes develop later in the day	15
Weak developing	No observed precipitation No radar echoes during budget interval Radar echoes appear shortly after the end of the budget interval	7
Moderate	No observed precipitation Radar echoes present during budget interval	5
Precipitating	Observed precipitation Radar echoes present during budget interval	12

* Budget interval: time period between two successive sets of rawinsonde ascents.

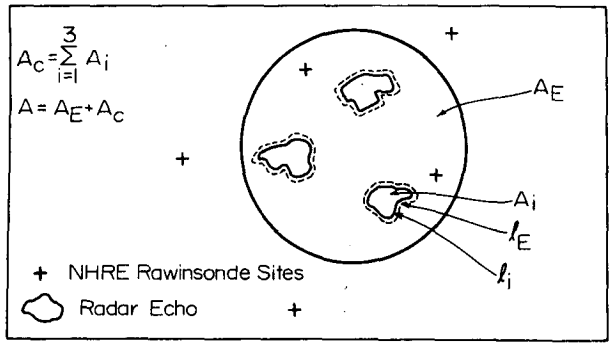

FIG. 3. Budget area decomposition.

within the 50 km radius budget area during the time interval defined by two sets of rawinsonde ascents.

A more detailed analysis of the radar and precipitation data was carried out and included a count of the number of echoes in each of three size (horizontal area) categories and a quantitative estimate of the total precipitation within the budget area. However, this analysis is not used because the accuracy of the additional quantitative detail is of the same order of magnitude as the neglected and/or modeled terms in the budget equation. Also, the division of the radar echo data into finer categories drastically reduces the number of data intervals in each category.

3. Budget equation

A budget calculation is straightforward to carry out, but the interpretation of the results is not straightforward. In this section and in Section 4 we attempt to clarify the interpretation of budget results by presenting the derivation of the budget equation used in this research. Also, two approximations related to the rapid time changes and large horizontal gradients that sometimes occur over the NHRE area are discussed. These approximations have not been discussed in previous budget studies.

The budget equation for the scalar χ over a time interval t_1 to t_2 and over a layer with area A and depth σ_1 to σ_2 is

$$\underbrace{\int_A\int_\sigma \pi\chi\Big]_{t_1}^{t_2} d\sigma dA}_{1} + \underbrace{\int_t\int_A\int_\sigma \nabla_\sigma\cdot(\pi\chi\mathbf{V})d\sigma dA dt}_{2} + \underbrace{\int_t\int_A \pi\chi\dot{\sigma}\Big]_{\sigma_1}^{\sigma_2} dA dt}_{3} = \int_t\int_A\int_\sigma \pi S d\sigma dA dt, \quad (1)$$

where $\sigma = p/\pi$, π is the surface pressure, S the source per unit mass of χ, and the notation $\Big]_{t_1}^{t_2}$ and $\Big]_{\sigma_1}^{\sigma_2}$ means evaluation at the limits t_1, t_2 and σ_1, σ_2. Normalized pressure σ has been chosen as the vertical coordinate for computational convenience, because the ground is the coordinate surface $\sigma = 1.0$. The hydrostatic approximation is used even though we are interested in studying convection, because the time and space scales of nonhydrostatic effects are probably much smaller than the integration scales A and $t_2 - t_1$. Area A is the circular area with a radius of 50 km over which we assume the data to be valid. Similarly, $t_2 - t_1$ is the 2–3 h interval between two successive sets of rawinsonde observations and $\sigma_2 - \sigma_1$ is the 0.01 (8–9 mb) vertical interval to which the sonde data have been interpolated.

We next introduce the main assumptions used in this budget study. The clear air (environmental) values of q, T and $\mathbf{V}$ are assumed to vary smoothly across the mesoscale data network, and the major perturbations to these background fields are caused by small, localized disturbances related to cumulus clouds. The smooth environmental fields are assumed to be well resolved by two successive sets of four or five rawinsonde measurements. These assumptions are incorporated into (1) in the following manner.

We conceptually divide the area of integration A into A_E and

$$A_c = \sum_i^N A_{ci}$$

(Fig. 3). The A_{ci} are the individual areas of the N clouds within area A. A_E is the environmental area between the clouds at any given moment. In area A_E the quantities q, T and $\mathbf{V}$ are set equal to the linear (plane) approximations discussed in Section 2b. This area decomposition is introduced into (1) and the resulting terms are arranged to separate the known quantities (χ_E and the total area A) from the unknown quantities (χ_{c_i} and A_i).

Term 1 of Eq. (1) becomes

$$\int_A\int_\sigma \pi\chi\Big]_{t_1}^{t_2} d\sigma dA = \underbrace{\int_A\int_\sigma \pi\chi_E\Big]_{t_1}^{t_2} d\sigma dA}_{1a} + \underbrace{\int_{A_c}\int_\sigma \pi(\chi_c-\chi_E)d\sigma dA_c\Big]_{t_1}^{t_2}}_{1b}.$$

In term 1a the integration of χ_E is taken over the total area A by simply extending the linear variation of χ_E into the cloud areas. In term 1b the integration over all the cloud areas,

$$\sum_{i=1}^{N}\int_{A_{ci}} (\,)dA_{ci},$$

is written as

$$\int_{A_c} (\,)dA_c.$$

Term 1b is the time change of the excess storage of χ

due to clouds. This term will be discussed in Sections 4 and 6.

Term 2 becomes

$$\int_t \int_A \int_\sigma \nabla_\sigma \cdot (\pi \chi \mathbf{V}) d\sigma dA dt = \int_t \int_A \int_\sigma \nabla_\sigma \cdot (\pi \chi \mathbf{V})_E d\sigma dA dt.$$

Only environmental quantities (subscript E) appear in this term. The term was derived by using the divergence theorem and assuming the common cloud-environment boundaries (Fig. 3) could be drawn close enough to each cloud so that the area A_c enclosed is approximately the cloud area and yet far enough away from the cloud so that the cloud properties become equal to the environment. This is related to the basic assumption of the study that clouds are small, localized perturbations to environmental fields. The presence of clouds on the outer boundary of A_E has been neglected. Such clouds would only produce a contribution to the budget if there is a net inflow or outflow of the local excess of χ during the period of the integration. The radar data show no net inflow of large clouds into the budget area. As in term 1, the integration is taken over the total area A by simply extending the linear variation of the environmental quantities into the cloud areas.

Some manipulation (addition and subtraction of the same term) is needed to obtain the desired expression for term 3. For simplicity we first consider only the area integration

$$\int_A \chi \pi \dot{\sigma} dA = \underbrace{\int_{A_E} \chi_E (\pi \dot{\sigma})_E dA_E}_{3a} + \underbrace{\int_{A_c} \chi_c (\pi \dot{\sigma})_c dA_c}_{3b} + \underbrace{\left(A_E^{-1} \int_{A_E} \chi_E dA_E\right)\left(\int_A \pi \dot{\sigma} dA\right)}_{3c} - \left(A_E^{-1} \int_{A_E} \chi_E dA_E\right)\left[\int_{A_E} (\pi \dot{\sigma})_E dA_E + \int_{A_c} (\pi \dot{\sigma})_c dA_c\right].$$

The decomposition of the third term into only an environmental term 3a and a cloud term 3b is not useful because the vertical mass flux $\pi \dot{\sigma}_E$ of the environment is not resolved by the measurements. Term 3c is introduced to solve this problem. Combining terms we obtain

$$\int_A \chi \pi \dot{\sigma} dA = \underbrace{\left(A_E^{-1} \int_{A_E} \chi_E dA_E\right)\left(\int_A \pi \dot{\sigma} dA\right)}_{3e} + \underbrace{\left[\int_{A_E} \chi_E (\pi \dot{\sigma})_E dA_E - \left(A_E^{-1} \int_{A_E} \chi_E dA_E\right) \int_{A_E} (\pi \dot{\sigma})_E dA_E\right]}_{3f} + \underbrace{\int_{A_c} \left[\chi_c - \left(A_E^{-1} \int \chi_E dA_E\right)\right] (\pi \dot{\sigma})_c dA_c}_{3g}.$$

The basic assumption stated at the beginning of this section has now been introduced. Term 3 is broken into a resolved part (3e) that is available from the measurements, and an unresolved part [(3f)+(3g)] that remains to be interpreted.

The source term S on the right-hand side (RHS) of (1) represents the gain or loss of χ by transformation processes. The particular processes operating in a budget depend on the budget quantity χ. In Section 4 we discuss the three thermodynamic quantities for which we compute budgets. For now we simply combine S with the unresolved portions of terms 1, 2 and 3.

Adding the time integration to term 3, defining the sum of the resolved terms as Q, and moving the unresolved terms to the RHS of the equation, we obtain

$$A(t_2 - t_1) \int Q_\chi \frac{\pi d\sigma}{g} = \int\int\int \pi S \frac{d\sigma}{g} dA dt - g^{-1} \int_t \left[\int_{A_E} \chi_E (\pi \dot{\sigma})_E dA_E + \left(A_E^{-1} \int_{A_E} \chi_E dA_E\right) \int_{A_E} (\pi \dot{\sigma})_E dA_E\right]_{\sigma_2}^{\sigma_1} dt - g^{-1} \int_t \left[\int_{A_c} \left(\chi_c - \left(A_E^{-1} \int_{A_E} \chi_E dA_E\right)\right) (\pi \dot{\sigma})_c dA_c\right]_{\sigma_2}^{\sigma_1} dt - \int_{A_c} \int_{\sigma_1}^{\sigma_2} \left[\pi (\chi_c - \chi_E) \frac{d\sigma}{g} dA_c\right]_{t_1}^{t_2}, \quad (2)$$

where

$$A(t_2 - t_1) \int Q_\chi \frac{d\pi\sigma}{g} \equiv \int_A \int_\sigma \pi \chi \Big]_{t_1}^{t_2} \frac{d\sigma}{g} dA + \int_t \int_A \int_\sigma \nabla_\sigma \cdot (\pi \chi V)_E \frac{d\sigma}{g} dA dt + g^{-1} \int_t \left[\left(A_E^{-1} \int_{A_E} \chi_E dA_E\right)\left(\int_A \pi \dot{\sigma} dA\right)\right]_{\sigma_2}^{\sigma_1} dt.$$

TABLE 3. Budget quantities.

χ	S
Total water mixing ratio $q=q_v+q_l$	None
Moist static energy $h=c_pT+gz+Lq_v$	r
Liquid water static energy $s_l=c_pT+gz-Lq_l$	r

r=radiation heating, q_v=water vapor mixing ratio, L=latent heat of condensation, q_l=liquid water mixing ratio.

The "apparent source" per unit mass Q_χ contains only resolved terms and they are calculated from the rawinsonde data. The results of the budget calculations are vertical profiles of Q_χ for each budget quantity χ. The terms in the RHS of (2) describe the unresolved processes that combine to produce the observed apparent source. The discussion of these processes is more straightforward if the budget quantity χ is specified because the source term S depends on the choice of χ.

The least well-known resolved quantity is the average vertical mass flux $\int\pi\dot{\sigma}dA$. As previously mentioned, it is forced to zero at the highest data level. In the results section we will compare vertical mass fluxes for the four categories of convection used in this study and also contrast the results with vertical velocities calculated in other budget studies. This latter comparison presents a slight problem because the NHRE terrain has a considerable slope [40 mb (100 km)$^{-1}$ in the east–west direction] compared to the lower boundaries (oceans) of the other studies. If vertical velocities with respect to pressure surfaces (ω) are compared, there will always be some built-in difference related to the sloping terrain and not related to the convection. The following argument suggests that this difference can be partly accounted for by comparing $\pi\dot{\sigma}$ of this research to ω values of other studies.

In studying convection it is reasonable to consider vertical velocities relative to surfaces that are nearly parallel to the cloud-base level. Pressure surfaces are appropriate over areas with level lower boundaries.

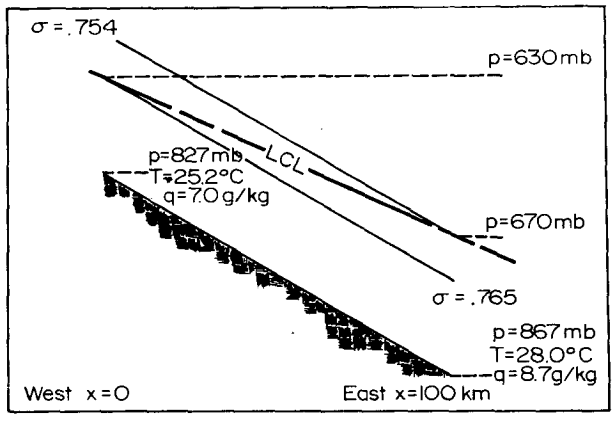

FIG. 4. Schematic east–west cross section of NHRE area (slope exaggerated).

The schematic east–west cross section of Fig. 4 uses average values of p, T and q to show the relation between p, σ and cloud-base (LCL) surfaces over the NHRE area. The cloud bases are nearly parallel to the σ surfaces, not p surfaces. Consequently, $\pi\dot{\sigma}$ is a velocity nearly relative to cloud bases over the NHRE area just as ω is a velocity nearly relative to cloud bases over level areas.

This argument begins to break down at high levels, because p surfaces begin to slope less with respect to σ surfaces. Also, the significance of the cloud base as a reference level becomes questionable at high levels. Fortunately, the difference between $\pi\dot{\sigma}$ and ω is relatively large only in the case of weak suppressed convection that does not reach high levels. Both $\pi\dot{\sigma}$ and ω profiles are presented in Section 5.

4. Apparent source

We have calculated budgets for thermodynamic quantities related to cumulus convection. In particular, the budget quantities are 1) total water mixing ratio, 2) moist static energy and 3) liquid water static energy. Betts (1975) presents a discussion of these quantities and the fundamental role they play in cumulus convection. Table 3 summarizes the definitions of these quantities and their related source terms.

Only two of the three quantities are independent, because the third can be obtained by combining the other two. Although q_l is not available from rawinsonde data, the apparent source can be calculated because q_l is zero in the environment, i.e., $q_{env}=q_v$ and $s_{l_{env}}=c_pT+gz$. The radiation source term

$$\int\int\int \pi r d\sigma dA dt \equiv Q_r$$

can be modeled from the measured values of q_v and T (plus assumed CO_2 and O_3). In Section 5 we show that Q_r is small in the case of weak convection and we assume it makes a negligible contribution to the budgets for moderate and precipitating convection. In the following discussion we treat Q_r as a known quantity.

Having chosen the budget quantities χ, we now proceed with the interpretation of the unresolved processes that combine to produce Q_q, Q_h-Q_r and $Q_{s_l}-Q_r$. Consider the q budget for example. Adding and subtracting

$$\int_{A_c} q_E(\pi\dot{\sigma})_c dA_c$$

to the apparent source, where

$$\int_{A_c} \text{represents} \sum_{i=1}^{N} \int_{A_i}$$

and the appropriate value of q_E is obtained by extending the linear variations of the environmental quantity q_E into each cloud area, yields

$$\int Q_q \frac{\pi d\sigma}{g} = \left\{ -\int_t \left[\int_{A_c} (q_c - q_E)(\pi\dot{\sigma})_c dA_c \right]_{\sigma_1}^{\sigma_2} dt \right.$$

$$-\int_{A_c}\int_{\sigma} [\pi(q_c - q_E) d\sigma dA_c]_{t_1}^{t_2}$$

$$\left. -\int_t \int_A \left[\left(q_E - \left(A_E^{-1} \int_{A_E} q_E dA_E \right) \right) (\pi\dot{\sigma}) \right]_{\sigma_1}^{\sigma_2} dA dt \right\}$$

$$\times [A(t_2 - t_1)] g^{-1}. \quad (3)$$

Instead of the difference

$$\left[\chi_c - \left(A_E^{-1} \int_{A_E} \chi_E dA_E \right) \right]$$

in (2) we have the difference $(q_c - q_E)$ in the first term of (3). Both q_c and q_E pertain to total water mixing ratio in the immediately around the ith cloud, but the subscript i is omitted because the notation is cumbersome. The difference $(q_c - q_E)$ is the local excess of q_c in a cloud over the nearby environmental value of q_E, and is a more useful quantity than the difference of q_c over an average value of q_E. See Fig. 5 for a schematic description of these two differences.

The third term on the RHS of (3) is a measure of the correlation of the vertical velocities in area A with the deviation of the environmental value q_E from the average value of q_E. The term can also be viewed as a measure of how "evenly" the clouds are distributed over the budget area. We assume that this correlation is nearly zero and neglect the third term in the interpretation of the apparent source profiles.

The usefulness of a local cloud excess $(q_c - q_E)$ and the possibility of a contribution of the third term in (3) are consequences of substantial horizontal gradients of q_E. These considerations were not necessary in the majority of previous budget studies which were performed over oceanic regions. However, Augstein *et al.* (1973) and Reed and Recker (1971) did take care to state that their analysis procedure implies horizontally linear changes of the mass flux as well as of other meteorological values. Also, Yanai *et al.* (1973) point out that their data region could be too large to properly represent the required averages because of substantial horizontal variations of large-scale parameters and because of the existence of short-lived mesoscale convective regions. Ninomiya (1974) remarked that he used mesoscale data because cumulus clouds are not always distributed uniformly over a large area.

The second term on the RHS of (3) is the time change of the excess storage of q due to clouds. It is usually neglected because A_c is small compared to A (typically 1–10%) and fairly constant in time. We neglect this term in the interpretation of the budgets calculated for weak suppressed, moderate and precipitating convection. However, it is retained in the interpretation of budgets calculated during periods of rapidly developing convection ("weak developing" category described in Section 2b).

Using the same approximations (including the neglect of the cloud storage term) as above, we obtain the following forms for the apparent sources of h and s (Q_q is included for completeness):

$$\int (Q_h - Q_r) \frac{\pi d\sigma}{g}$$

$$= -(ATg)^{-1} \int_t \left[\int_{A_c} (h_c - h_E)(\pi\dot{\sigma})_c dA_c \right]_{\sigma_1}^{\sigma_2} dt$$

$$= -\int_{\sigma_1}^{\sigma_2} \frac{\partial}{\partial\sigma} [F_h] d\sigma, \quad (4)$$

$$\int (Q_{s_l} - Q_r) \frac{\pi d\sigma}{g}$$

$$= -(ATg)^{-1} \int_t \left[\int_{A_c} (s_{l_c} - s_{l_E})(\pi\dot{\sigma})_c dA_c \right]_{\sigma_1}^{\sigma_2} dt$$

$$= -\int_{\sigma_1}^{\sigma_2} \frac{\partial}{\partial\sigma} [F_{s_l}] d\sigma, \quad (5)$$

$$\int Q_q \frac{\pi d\sigma}{g}$$

$$= -(ATg)^{-1} \int_t \left[\int_{A_c} (q_c - q_E)(\pi\dot{\sigma})_c dA_c \right]_{\sigma_1}^{\sigma_2} dt$$

$$= -\int_{\sigma_1}^{\sigma_2} \frac{\partial}{\partial\sigma} [F_q] d\sigma, \quad (6)$$

where

$$T \equiv (t_2 - t_1), \quad F_h \equiv \int_{\sigma_t}^{\sigma} (Q_h - Q_r) \frac{\pi d\sigma}{g},$$

and σ_T is the top of the convective layer where F_h is set equal to zero. F_{s_l} and F_q are similarly defined.

The three convective flux quantities F_h, F_{s_l} and F_q have been thoroughly discussed by Betts (1975). We present the results (Section 6) of the budget calculations in the source form (Q_q, $Q_h - Q_r$ and $Q_{s_l} - Q_r$) and also

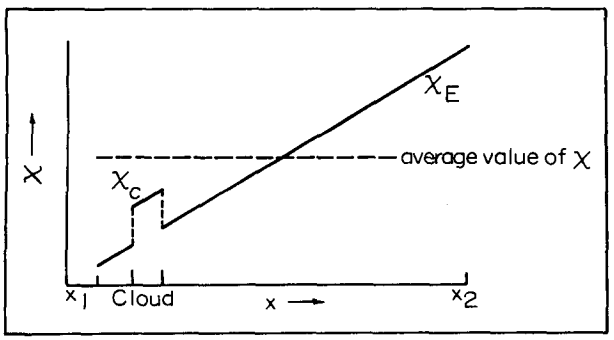

FIG. 5. Schematic representation of χ_E with a large horizontal gradient.

as vertical fluxes (F_q, F_h and F_{s_l}). The use of total water mixing ratio and liquid water static energy as budget quantities has resulted in the explicit absence of a source term S for condensation/evaporation. These processes are now implicitly present as the vertical convergence/divergence of the liquid water portion of F_q and F_{s_l}. The use of these fluxes as a method to present budget results is formally correct for both the nonprecipitating and precipitating convection categories. However, the interpretation of these profiles is much more straightforward in the case of nonprecipitating convection.

In the precipitating case q and s_l are no longer parcel quantities and the part of the liquid water portions of q and s_l associated with the falling precipitation does not move with the parcel velocity associated with q_v or c_pT+gz. We could have described the precipitation falling relative to a parcel as an unknown sink of liquid water, but we include it as an unknown flux of liquid water because water is being lost by crossing a boundary.

Eqs. (4), (5) and (6) are based on the assumption that observations resolve smooth environmental fields of q, T and $\mathbf{V}$ and that dry and moist convection produces localized perturbations in these fields. The divergence of vertical transports associated with convective velocities, $\pi\dot{\sigma}_c$, and cloud-environment differences produce the calculated apparent sources of moisture and energy. Furthermore, the space integration

$$\int_A ( )dA_c \equiv \sum_i \int ( )dA_{ci}$$

emphasizes the fact that the calculated apparent sources pertain to the net contribution of all the clouds in the budget volume. The time integration shows that we are dealing with the contribution of each cloud integrated over its entire life cycle.

Average apparent sources for three categories of convection are presented in the next section. Organizing and comparing budget results in terms of radar/precipitation characteristics of the convection is one way to extend the interpretation of the results beyond the general discussion presented above. In Section 6 the interpretation of the "weak developing" category results is taken farther with the use of a very simple model.

5. Results

The apparent sources of q, h and s_l presented in this section are averages of individual budgets calculated for the weak suppressed, moderate and precipitating categories described in Section 2b. The budgets for s_l and h involve a radiation source term Q_r which we were able to calculate for the case of weak suppressed convection. Dr. S. K. Cox kindly supplied longwave and shortwave computer programs to calculate Q_r using a combination of observed and standard atmosphere values of T, q_v, CO_2 and O_3. The longwave program uses synoptic estimates of cloud-base, cloud-top and fractional coverage to account for the effects of clouds. The shortwave program assumes a clear sky. This is tolerable in the case of weak suppressed convection because the cloud cover is small. However, the trial Q_r profiles for moderate and precipitating categories are not used because the larger cloud cover cloud not be ignored in the shortwave calculations.

The magnitude of Q_r (Fig. 6) for the weak suppressed category is about one-tenth of the magnitude of the apparent sources of s_l and h. We do not have acceptable

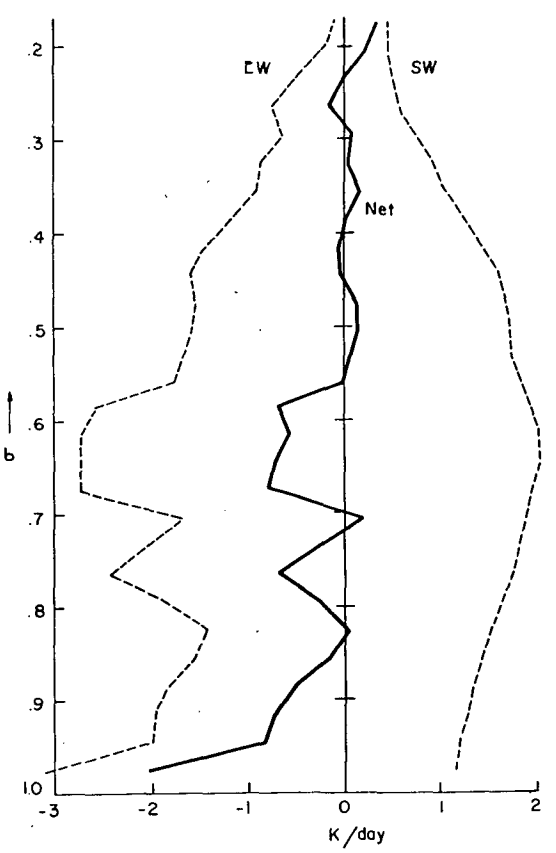

FIG. 6. Radiation source—weak suppressed convection.

model values of Q_r for the moderate and precipitating categories, but based on the results of the weak suppressed case we assume Q_r is negligible in these two cases.

The results of the budget calculations are presented as convective flux profiles and diagrams summarizing the total subcloud layer and cloud layer apparent sources. The flux profiles are obtained by integrating (4), (5) and (6) downward from the estimated top σ_T of the cloud layer. In the case of moderate and precipitating convection the cloud layer top is taken as the approximate tropopause level, $\sigma_T=0.30$ (250 mb). Above this σ_T the calculated Q_h and Q_{s_l} become large and erratic due to inaccuracies in the upper level rawinsonde winds. In the case of weak suppressed convection the top of the cloud layer is set to $\sigma_T=0.50$ (430 mb). This subjective estimate of the maximum cloud-top height is consistent with the shallow, nondeveloping nature of the cumulus clouds in this category. The convective fluxes are set to zero at and above σ_T.

The choice of σ_T has a large influence on the magnitude of the convective fluxes but does not alter the slope of the profile below σ_T. The bulk of the information contained in a flux profile is related to the slope, not the magnitude, of F because the apparent source is the vertical derivative of F. The magnitude of F at a particular level is a measure of the total apparent source above that level. The following rough checks can be made on the surface magnitudes of F_h and F_q. A simple energy balance at the ground shows $F_h(\text{sfc}) \approx F_r(\text{sfc})$ if ground storage is neglected. F_r is the net radiation flux and is available from the radiation programs used to calculate Q_r. A calculation for a clear sky gives $F_r(\text{sfc})=725$ W m^{-2}. This value is an upper bound for $F_h(\text{sfc})$. Similarly, a surface water budget gives $F_q(\text{sfc})=$ evaporation-precipitation. Although sufficiently accurate estimates of precipitation and evaporation (including substantial evapotranspiration) are not available, the calculated surface value of F_q can be checked in a qualitative manner.

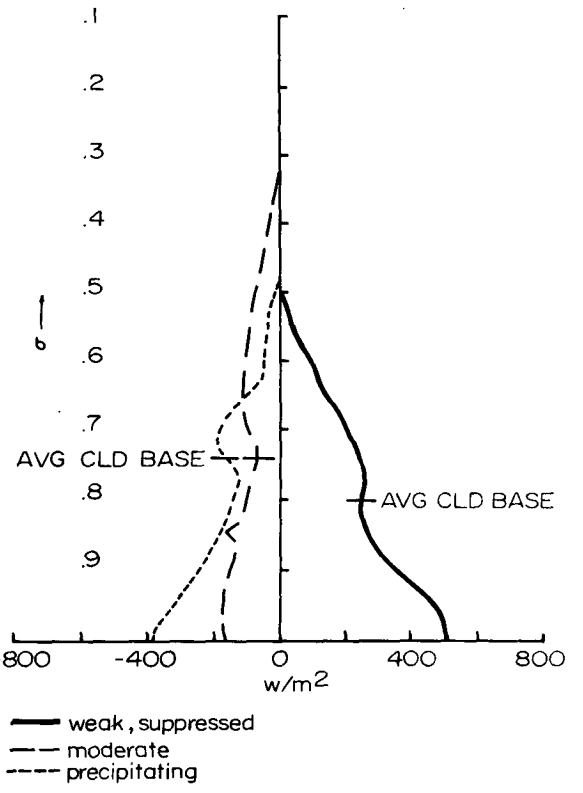

FIG. 8. Convective flux of total water (F_q) times latent heat of condensation (L).

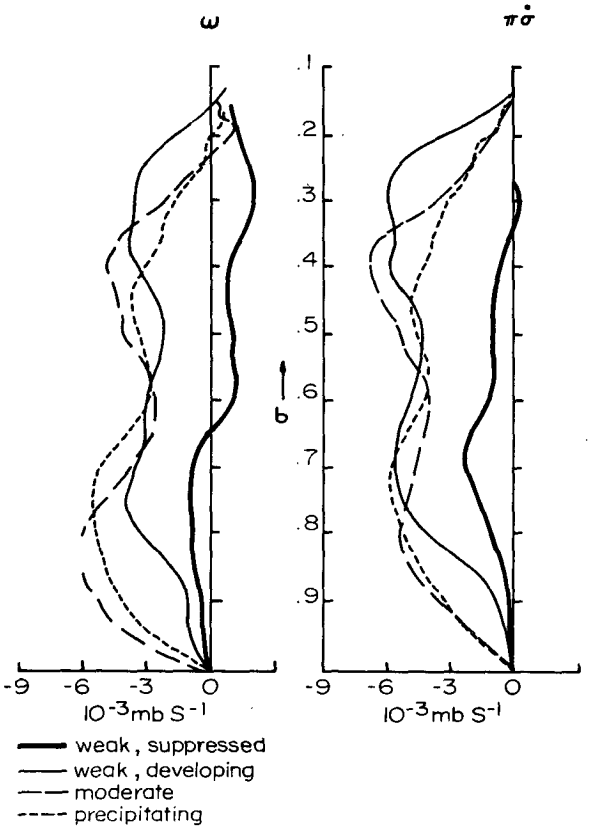

FIG. 7. Average vertical mass flux.

The average vertical mass flux profile [either $\pi\dot{\sigma}$ or ω (see Fig. 7)] for weak suppressed convection shows a surprising upward motion below cloud base. This is a distinct difference compared to the suppressed convection of the previously mentioned studies ("undisturbed" BOMEX, "weak/absent" ATEX, "region 8" of Reed and Recker, and "no echo" of Ninomiya). The individual suppressed cases show both ascending and descending layers, but the subcloud descent is lost in the averaging. In almost every individual weak suppressed case there is a layer of net descending air either above cloud top or below cloud base that is compatible with the observed lack of development of the clouds.

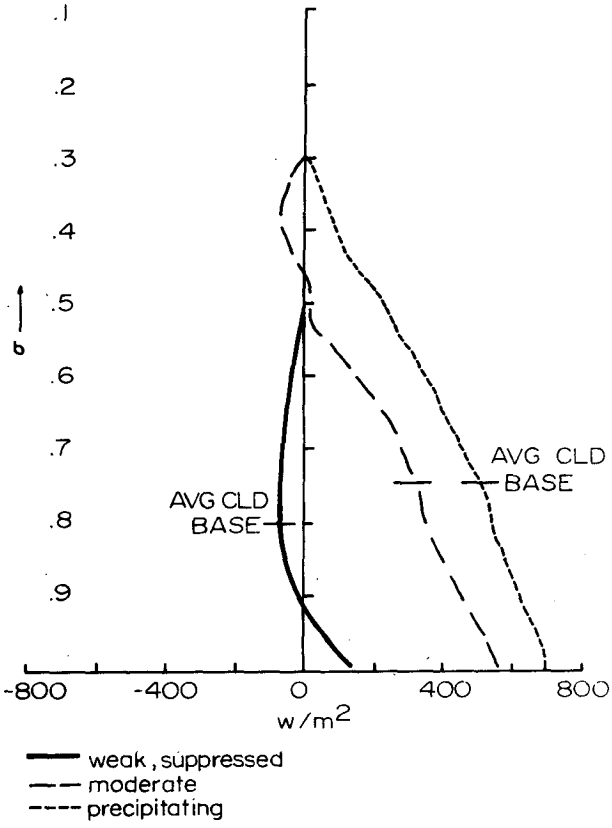

FIG. 9. Convective flux of liquid water and static energy (F_{s_l}).

Developing, moderate and precipitating convection averages (Fig. 7) show a second type of $\pi\dot{\sigma}$ profile. The net vertical motion is ascending and the ascent profiles have a double maximum. The lower maximum near cloud base occurs not only in the average, but is also present in many of the individual profiles. Several other mesoscale studies (Fankhauser, 1969; Lewis, 1975; Betts, 1973) have shown this double maximum. It is not present in previous large-scale studies. This double maximum in the average vertical mass flux profile may, therefore, be a characteristic feature of mesoscale circulations containing deep convection.

The convective flux profiles of LF_q, F_{s_l} and F_h are presented in Figs. 8, 9 and 10.

The surface value of the convective flux of total water is equal to the net source or sink of water in the budget volume. Fig. 8 shows that F_q(sfc) relates qualitatively well to the type of convection present in the weak, moderate and precipitating categories. The positive value in the weak convection case indicates an evaporation of water at the rate of 0.07 cm h^{-1}. This evaporation rate is large compared to the 0.01–0.05 cm h^{-1} rate calculated over the previously mentioned oceanic areas. However, considering that the air near the ground in the NHRE area was very hot and dry (37°C and 8 g kg^{-1} compared to 28°C and 18 g kg^{-1} in the BOMEX case), it is quite reasonable to expect more vigorous evaporation processes in this situation. Similarly large evaporation rates (0.04 cm h^{-1} daytime mean and 0.05–0.06 cm h^{-1} midafternoon values) have been calculated from the Great Plains Turbulence Field Program data [Tables 7.3.1 and 7.3a in Lettau and Davidson (1957)]. These data were taken in open prairie country near O'Neill, Nebraska, during August and September.

The moderate and precipitating cases show successively larger net sinks of water (−0.02 and −0.05 cm h^{-1}) associated with increasing precipitation. The small negative value in the moderate case stands opposed to the "no observed precipitation" criterion of the moderate category. However, radar echoes are observed in the moderate category. The calculated −0.02 cm h^{-1} is likely to be a combination of error plus unobserved precipitation.

The surface value of the convective flux of moist static energy is equal to the net radiation at the ground. F_r(sfc) is a maximum with clear skies and decreases as the cloudiness increases. The decrease in the calculated surface flux of h (Fig. 10) from F_h(sfc) = 603 W m^{-2} for weak to 383 W m^{-2} for moderate to 305 W m^{-2} for precipitating categories is qualitatively consistent with the increasing cloudiness characteristic of these categories. The magnitude of F_h(sfc) in the

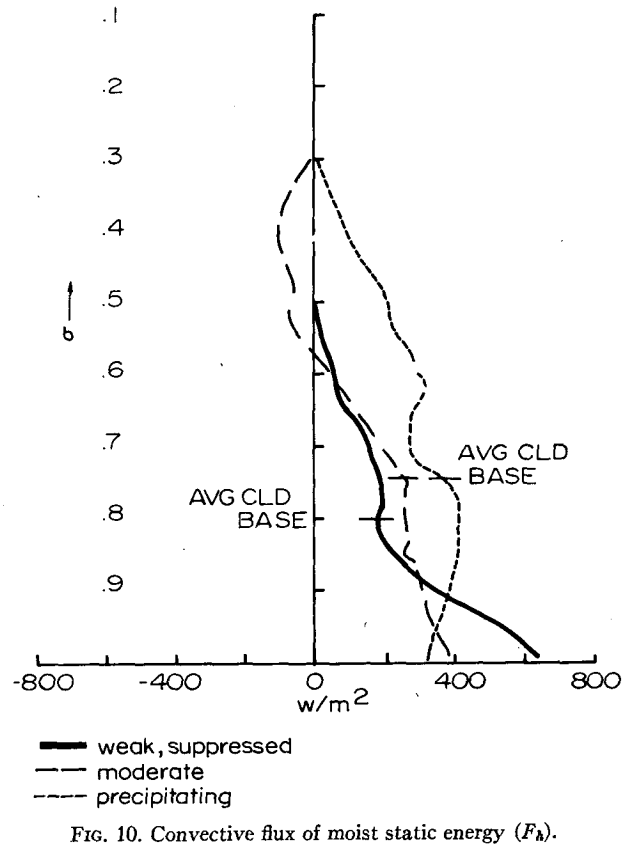

FIG. 10. Convective flux of moist static energy (F_h).

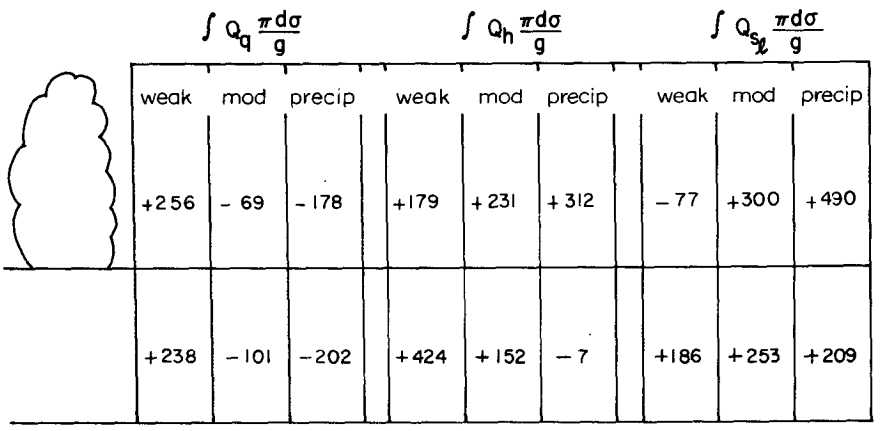

FIG. 11. Apparent sources (W m^{-2}) of q, h and s_l for cloud and subcloud layers.

weak convection category is reasonably less than the modeled 725 W m^{-2} clear sky net radiation.

In the weak convection category part of the water that is available from surface evaporation appears as an apparent source of water vapor in the subcloud layer (Fig. 11). It is distributed throughout this layer by dry convection and mechanical mixing. In contrast, the moderate and precipitating categories show an apparent sink of water vapor in the subcloud layer. This drying cannot be due to a loss of water vapor by condensation. Rather, it is due to the introduction of dry air in the subcloud layer by convection processes. Such apparent sinks of water vapor are also present in Ninomiya's (1974) "echo cluster" budgets, the Reed and Recker (1971) trough region data, as discussed by Cho and Ogura (1974), the midlatitude squall line budget calculations of Lewis (1975), and the mesoscale cumulonimbus budget of Betts (1975).

Betts (1976) relates the subcloud drying to downdrafts. The downdrafts are modeled as originating above cloud base and are driven and moistened by evaporating precipitation. However, the descending air is originally so dry that it remains dry relative to the subcloud air and consequently appears in a budget calculation as an apparent sink.

Weak, moderate and precipitating convection all produce apparent sources of s_l in the subcloud layer (Fig. 11). This can be interpreted as a warming or addition of dry static energy (c_vT+gz) because q_l is zero. The processes involved are dry convection and mechanical mixing. The magnitude of this warming is about the same for all three categories of convection. This means that the previously mentioned downdrafts produce little cooling compared to the subcloud convective heating processes.

The apparent source of moist static energy (Fig. 11) in the subcloud shows the combined result of convective sources of dry static energy and water vapor. Dry thermals and mechanical mixing in the layer below weak, suppressed cumulus clouds produce a strong apparent source of h throughout the subcloud layer. As the intensity of the convection increases to moderate and then to precipitating, the convective heating remains approximately constant, but the introduction of dry air produces a smaller source and finally an apparent sink of h. Previously mentioned studies also show this apparent subcloud sink of h for budgets calculated during disturbed conditions.

In the cloud layer the discussion of the apparent sources of q and s_l must recognize the contributions due to liquid water transports (including condensation and evaporation). Discussion of the apparent source of h is somewhat simpler because the troublesome liquid water contribution is not explicitly present.

All three categories produce an apparent source of moist static energy in the cloud layer (Fig. 11). The generally positive slopes of the three average F_h profiles (Fig. 10) are present in the individual profiles that make up the average profiles. The positions of the layers showing apparent sinks (negative slope), however, are mostly a result of averaging. The shallow layers with zero or negative slopes do not consistently appear just above the cloud base as the average profiles indicate. Also, the upper level sink in the moderate case is likely to be noise.

Moist static energy is an approximately conserved quantity for both dry and moist processes. This means that the apparent source of h is due to cumulus clouds transporting and depositing the subcloud air with its relatively high values of h into the cloud layer.

In the case of weak convection this apparent source of h is composed of a source of q (Fig. 8) plus a sink of s_l (Fig. 9). The F_{s_l} profile shows that the sink of s_l occurs in the upper half of the cloud layer. It is surprising and perhaps questionable that the lower half of the cloud layer F_{s_l} profile shows only a very weak source of s_l. The slope of the upper half of F_{s_l} is readily interpreted as cooling due to evaporation of cloud water. There is not enough corresponding heating in the lower half of the layer to bring F_{s_l} to a near zero value at cloud base.

In the moderate and precipitating cases the roles of

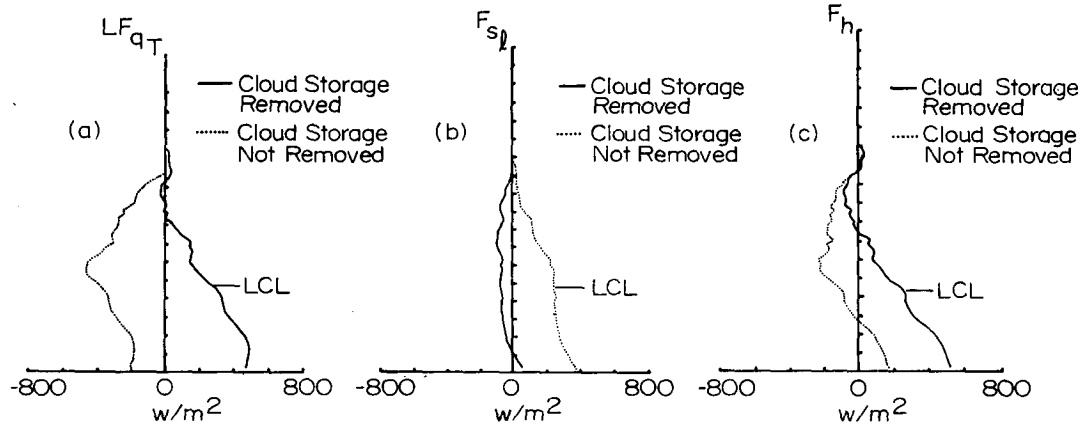

FIG. 12. Flux representation of the apparent sources of Lq, s_l and h with cloud storage removed (solid lines) and without cloud storage removed (dotted lines).

q and s_l fluxes are the opposite of those described for the weak convection case. The convective addition of moist static energy to the cloud environment is due to an apparent source of s_l plus a sink of q. The apparent sink of water vapor in the environment is due to condensation and then loss of the liquid water by precipitation. The F_{s_l} profile is consistent with condensation heating. The liquid water that is lost by precipitation comes from two sources. One is simply that the cloud-base updrafts contain saturated subcloud air that eventually condenses in the cloud. If this were the only source of water vapor to be condensed, the F_q profile would show no apparent source or sink in the cloud layer. The presence of an apparent sink of moisture means that convective processes are replacing environmental air with air that is dry relative to the environment. Calculations of Cho and Ogura (1974), Ninomiya (1974), Betts (1975) and Lewis (1975) also show this cloud layer apparent sink of water vapor for budget areas containing precipitating convection.

It is necessary to introduce cloud models in order to gain a clearer picture of the processes that produce these various convective flux profiles. Such models quantitatively describe the transports produce by the cumulus clouds. The budget calculations can be used either to close the models or to check the internal consistency of the models [see Betts (1975) for a discussion of the relation between models and budgets]. In the next section we use a simple cloud model plus the results of the budget calculations for weak developing convection to investigate the cloud storage of water and static energy.

6. Cloud storage

The change of cloud storage was derived in Section 4 as part of the apparent source term. This term was neglected in the discussion of the results for weak suppressed, moderate and precipitating convection because the cloud area A_c was small and was not changing rapidly with time. The term is not negligible, however, for budget periods with weak developing convection. The cumulus clouds in this category produce no radar echoes during the budget period, but echoes and/or precipitation appear shortly after (within 2 h) the end of each budget period.

The average apparent sources of q, s_l and h were calculated for the weak developing category and "convective fluxes" were derived from these source calculations with $\sigma_T = 0.40$ and with no attempt to account for cloud storage (dotted profiles in Fig. 12). The F_q profile offers the clearest indication that the cloud storage term is not negligible for developing convection. The negative slope of F_q throughout the cloud layer indicates an apparent sink of moisture and the negative surface value of F_q means that there is a net loss of water in the budget volume. This sink is not due to precipitation because the clouds in this category do not even produce radar echoes during the budget period. It is reasonable to ascribe the net loss of water vapor to an increase in the number and/or size of the clouds in the budget volume. The dotted "convective flux" profiles in Fig. 12 are really the sum of a convective flux plus a storage term.

We now use a simple model to calculate the cloud storage in terms of a vertical profile of the time change of the fractional cloud area $\Delta(A_c/A)/\Delta t$. The results of the budget calculations are used to close the model. Most important, the $\Delta(A_c/A)/\Delta t$ profile is calculated twice, once making use of the q budget results and once making use of the s_l budget results to close the model. The quantities q and s_l are independent of each other (Section 4) and consequently the two different methods of closing the model will not necessarily produce similar $\Delta(A_c/A)/\Delta t$ profiles. However, the two derived profiles do turn out to be quite similar and this agreement gives some confidence that the cloud model is appropriate to use for calculations of cloud storage.

The first step in building this model is separating the cloud storage term from the apparent source which is the sum of a convective flux plus the cloud storage. To

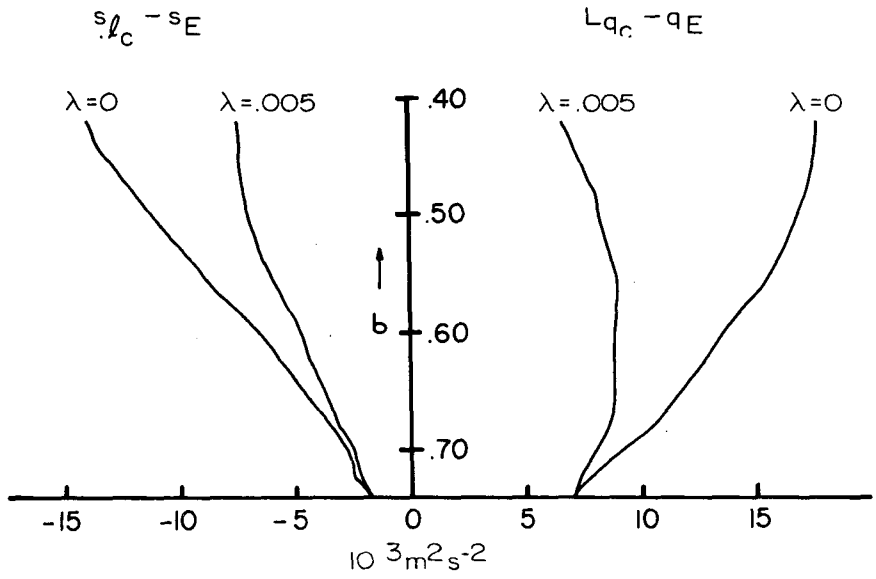

FIG. 13. Model cloud excess liquid water static energy and total water for $\lambda=0$, 0.005 mb^{-1}.

do this we make use of the convective flux profiles calculated for the suppressed case. We assume that both weak suppressed and weak developing convection produce equal convective transports of χ above cloud base. This is reasonable because both categories of weak convection are composed of small cumulus clouds that do not produce radar echoes during the budget period.

Subtracting the suppressed case F profiles from the developing case F profiles gives the total change of cloud storage:

$$\Delta F_q' = -(AT)^{-1}\int_A\int_{\sigma_1}^{\sigma_2}\left[\pi(q_c-q_e)\frac{d\sigma}{g}dA_c\right]_{t_1}^{t_2},$$

where

$$\Delta F_q' = \Delta F_q(\text{dev}) - \Delta F_q(\text{supp})$$
$$\Delta F_q = F_q(\sigma_2) - F_q(\sigma_1).$$

The vertical difference ΔF_q(dev) is proportional to the apparent source of q in the layer σ_2 to σ_1 for the weak developing category. $\Delta F_q'$ is equal to the developing minus suppressed apparent sources of q and is calculated by subtracting the F_q profile of Fig. 8 from the dotted profile of Fig. 12a. Because the suppressed and developing cloud bases are at slightly different levels, the suppressed (lower) convective profiles were raised 0.06 σ to make the cloud bases coincide before subtraction.

We next let (q_c-q_E) be representative values over area A_c, layer $(\sigma_2-\sigma_1)$ and period T [the usual bar ($\bar{}$) notation is omitted for clarity]:

$$\Delta F_q' = (q_c-q_E)(\pi\Delta\sigma/g)\left\{\frac{1}{T}\left[\left(\frac{A_c}{A}\right)_{t_2}-\left(\frac{A_c}{A}\right)_{t_1}\right]\right\}, \quad (7a)$$

$$\Delta F_{s_l}' = (s_{l_c}-s_E)(\pi\Delta\sigma/g)\left\{\frac{1}{T}\left[\left(\frac{A_c}{A}\right)_{t_2}-\left(\frac{A_c}{A}\right)_{t_1}\right]\right\}. \quad (7b)$$

Taking the (q_c-q_E) outside of the time and cloud area integrals means we are modeling the cloud storage effects of all the clouds in the budget volume with a single average cloud.

Finally, we specify this average cloud as a simple entraining parcel. The dilution of the conservative cloud properties q_c and s_{l_c} in the cloud is given by

$$\frac{\partial q_c}{\partial\sigma} = \lambda(q_c-q_E), \quad (8a)$$

$$\frac{\partial s_{l_c}}{\partial\sigma} = \lambda(s_{l_c}-s_E). \quad (8b)$$

The entrainment rate λ will be assumed. The cloud storage results do not depend critically on the choice of λ. The integration of (8a,b) requires vertical profiles of q_E and s_E (available from the rawinsonde data) and lower boundary values of q_c and s_{l_c} at cloud base. The boundary values are set equal to q and s at $\sigma=0.99$. This is consistent with the procedure used to calculate the average cloud-base height. The results of this integration (Fig. 13) are profiles of the local cloud-environment differences (q_c-q_E) and $(s_{l_c}-s_E)$. The two choices of λ (0 and 0.005 mb^{-1}) represent reasonably extreme values of entrainment for shallow convection.

Two independent estimates of the change of fractional cloud area

$$\Delta(A_c/A)/\Delta t = \frac{1}{T}\left[\left(\frac{A_c}{A}\right)_{t_2}-\left(\frac{A_c}{A}\right)_{t_1}\right]$$

are calculated from (7a,b). The agreement of these estimates [as given by the similarity of the (○) and (×) profiles of Figs. 14 and 15] does not depend strongly on the choice of λ. The use of $\lambda=0$ produces slightly

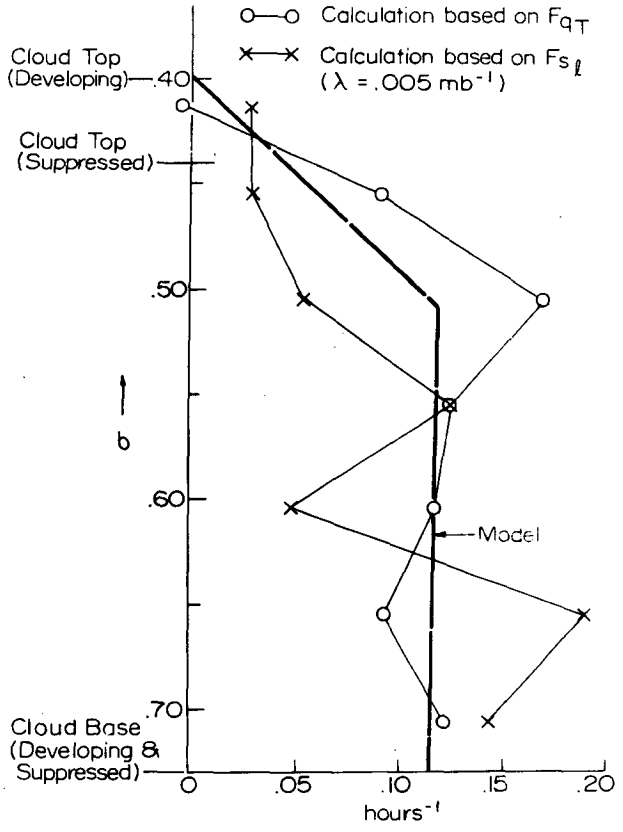

FIG. 14. Time change of fractional cloud area, $\lambda = 0.005$ mb^{-1}.

better agreement than the use of $\lambda = 0.005$ mb^{-1}. The approximate shape of the $\Delta(A_c/A)/\Delta t$ profiles (heavy dashed and solid lines in Figs. 14 and 15) is somewhat more dependent on the choice of λ.

Both profiles show a time change of fractional cloud area on the order of 0.1 h^{-1}. This is a substantial increase, but it is quite consistent with the general developing character of the convection and the fact that it represents development over about a 3 h period in the afternoon. The $\Delta(A_c/A)/\Delta t$ profiles calculated using q budget results agree within about 0.05 h^{-1} with the profiles calculated using s_l budget results. To complete the model of cloud storage we simply approximate the two derived profiles in Fig. 15 ($\lambda = 0$) by a single, linearly decreasing profile (solid line).

The final model of cloud storage is given by the linear $\Delta(A_c/A)/\Delta t$ profile of Fig. 15 and the $(q_c - q_E)$ and $(s_{l_c} - s_E)$ profiles of $\lambda = 0$ in Fig. 13. The model is used to subtract the cloud storage from the dotted F profiles of Fig. 12. The resulting solid profiles are convective fluxes with no storage contribution. The similarity of these solid F profiles and those for weak suppressed convection is another, although not independent, check that a parcel cloud model plus a single $\Delta(A_c/A)/\Delta t$ profile can be combined with budget data to give a reasonable estimate of cloud storage.

7. Summary and conclusions

Mesoscale rawinsonde data from the NHRE are analyzed throughout a cylindrical volume for use in budget calculations. The analysis approximates the data as linear functions of position and time in order to account for sonde drift and rise time. The average absolute differences between the original data and the linear approximations to the original data are on the order of the measurement errors associated with a GMD-1a rawinsonde system. The approximated horizontal velocities are further adjusted so that the calculated vertical velocities are zero at the highest data levels (~120 mb).

The radar and precipitation data for the budget volume are stratified so that the results of the budget calculations could be presented as average budgets for four classes of convection. The four classes of convection—weak, developing, moderate and precipitating—are very broad and involve only a distinction of whether or not precipitation and/or radar echoes were present within the budget volume.

A derivation of the budget equations for total water mixing ratio, moist static energy and liquid water static energy is presented. The environmental values of these budget quantities sometimes have large horizontal gradients across the NHRE area. These gradients introduce a budget equation term that is related to how "evenly" the clouds are distributed over

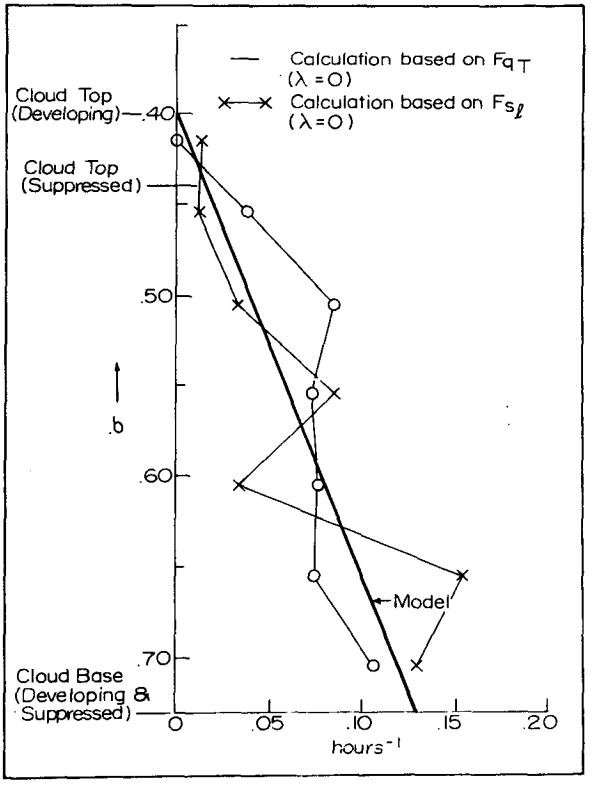

FIG. 15. As in Fig. 14 except $\lambda = 0$ mb^{-1}.

the budget area. We neglect this term in the interpretation of the budget results. The derivation also includes a change of cloud storage term. This term is neglected in the interpretation of the weak, moderate and precipitating budgets, but is very important in the case of developing convection.

The results of the budget calculations are presented as average convective flux profiles and also as apparent sources and sinks of the budget quantities in the subcloud and cloud layers. In weak convection cases there is an apparent source of water vapor in the subcloud layer due to dry convection and mechanical mixing. In contrast, the moderate and precipitating categories show an apparent sink of water vapor in the subcloud layer due to convective downdrafts. All the categories of convection warm the subcloud layer. The magnitude of this warming is about the same for each category. This means that the downdrafts produce little cooling compared to the subcloud heating processes.

All four categories of cumulus clouds produce an apparent source of moist static energy in the cloud layer by transporting and depositing the subcloud air with its relatively high values of h into the cloud layer. In the case of weak convection the lower half of the cloud layer is slightly warmed by condensation and the upper half of the cloud layer is cooled by evaporation. In the case of moderate and precipitating convection the entire cloud layer is warmed by condensation. The water vapor that falls out of the cloud layer as precipitation comes from both subcloud layer and cloud layer air. The loss of water vapor from the environmental air in the cloud layer means that convective processes are replacing environmental air with air that is dry relative to the environment.

Developing convection produces heating and a sink of water vapor due to a change of cloud storage that is larger than the sources and sinks due to convective transports of water and energy. A simple parcel model is used to calculate the cloud storage in terms of a vertical profile of the time change of the fractional cloud area. The results of the budget calculations for both total water and liquid water static energy are used to close the model. The general similarity of the two derived fractional cloud area change profiles gives some confidence that the cloud storage can be estimated using a simple model plus budget results.

Acknowledgments. This research was supported by the National Science Foundation and the GATE project office under NOAA Grant OCD74-21678, and with the additional support of National Science Foundation Grant ERT71-01885.

The authors are indebted to the National Hail Research Experiment personnel who supplied most of the data used in this research. We also thank Dr. Stephen Cox for supplying the radiation program, Richard Miller for assisting with the computer programming and Pauline Martin for the data reduction.

REFERENCES

Augstein, E., H. Riehl, F. Ostapoff and V. Wagner, 1973: Mass and energy transports in an undisturbed Atlantic trade-wind flow. *Mon. Wea. Rev.*, **101**, 101–111.

Betts, A. K., 1973: A composite mesoscale cumulonimbus budget. *J. Atmos. Sci.*, **30**, 597–610.

——, 1975: Parametric interpretation of trade-wind cumulus budget studies. *J. Atmos. Sci.*, **32**, 1934–1945.

——, 1976: The thermodynamic transformation of the tropical sub-cloud layer by precipitation and downdrafts. *J. Atmos. Sci.*, **33**, 1008–1020.

Cho, H. R., and Y. Ogura, 1974: A relationship between the cloud activity and the low-level convergence as observed in Reed-Recker's composite easterly waves. *J. Atmos. Sci.*, **31**, 2058–2065.

Fankhauser, J. C., 1969: Convective processes resolved by a mesoscale rawinsonde network. *J. Appl. Meteor.*, **8**, 778–798.

——, 1974: The derivation of consistent fields of wind and geopotential height from mesoscale rawinsonde data. *J. Appl. Meteor.*, **6**, 637–646.

Holland, J. Z., and E. M. Rasmusson, 1973: Measurements of the atmospheric mass, energy and momentum budgets over a 500-kilometer square of tropical ocean. *Mon. Wea. Rev.*, **101**, 44–55.

Lettau, H. H., and B. Davidson, 1957: *Exploring the Atmosphere's First Mile*, Vols. I and II. Pergamon Press.

Lewis, J. M., 1975: Test of the Ogura-Cho model on a prefrontal squall line case. *Mon. Wea. Rev.*, **103**, 764–778.

Ninomiya, K., 1974: Bulk properties of cumulus convections in the small area over Kurishio region. *J. Meteor. Soc. Japan*, **52**, 188–202.

Nitta, T., and S. Esbensen, 1974: Heat and moisture budget analyses using BOMEX data. *Mon. Wea. Rev.*, **102**, 17–28

O'Brien, J. J., 1970: Alternative solutions to the classical vertical velocity problem. *J. Appl. Meteor.*, **9**, 197–203.

Reed, R. J., and E. E. Recker, 1971: Structure and properties of synoptic scale wave disturbances in the equatorial Pacific. *J. Atmos. Sci.*, **28**, 1117–1133.

Yanai, M., S. Esbensen and J. Chu, 1973: Determination of average bulk properties of tropical cloud clusters from large-scale heat and moisture budgets. *J. Atmos. Sci.*, **30**, 611–627.